[1]Sheriff O. SAKA, [2]Saliu O. SEIDU, [3]Akeem D. AKINWEKOMI, [4]Akinlabi OYETUNJI

ALLOYING ELEMENTS VARIANT ON THE DEVELOPMENT OF ANTIMONY MODIFIED COMPACTED GRAPHITE IRON USING ROTARY FURNACE

[1-4]Department of Metallurgical and Materials Engineering, Federal University of Technology, Akure, NIGERIA

Abstract: In this study, the production and properties evaluation of compacted graphite iron (CGI) were experimented. Sand casting was employed in producing the CGI alloys using rotary furnace to melt the charges. Rod pattern was used to produce the CGI alloy samples with different alloying treatments. Alloy C is the unmodified CGI alloys while alloy A1, A2 and A3 are antimony Sb-modified CGI alloys at varying addition of 0.003, 0.006 and 0.05 wt% respectively. Mg and Ce FeSi treated alloy C; and Mg, Ce, Al, Cu, Sb – modified alloys were all subjected to mechanical tests according to ASTM standards. The chemical compositions were obtained using spectrometry analyzer. The microstructure of the samples was viewed using metallurgical optical microscope and analysed with image analyzer. The result of the chemical analysis of the CGI alloys produced solidified as hypoeutectic (for alloy samples C and A1) and hypereutectic (for A2 and A3) which showed a low silicon (1.66 – 1.76) % and high sulphur (0.110 – 0.147) contents of their respective Si/C and Mg/S ratios. The microstructure details revealed that increased antimony addition increases pearlite content and modified the compacted graphite particles from thick, short, and wormy – like with round - ended edges to less thick, short, wormy and crab – like graphite with needle and rough edges in pearlitic matrix interspersed with carbide. Mechanical properties (tensile, % elongation and elastic modulus) were improved as antimony addition increases particularly for alloy A1 while lowest values were within alloys C and A1. Alloy C has the highest average hardness of 87.4 HRA while Alloy A1 possessed the least value (83.2 HRA). Hence, alloy A2 has the best overall property which is between Grade 300 – 350 according to ASTM A842 – 85.

Keywords: Alloying element, Antimony, Compacted Graphite, Mechanical, Rotary furnace

1. INTRODUCTION

Compacted graphite irons (CGI) had been in existence long ago as a result of inadequacy of magnesium or cerium amounts in the melts which was intended to produce spheroidal graphite iron [1]; however, CGI was able to find itself in the family of cast iron since 1965 as a cast material possessing intermediate mechanical and physical properties which fall between spheroidal and grey cast irons respectively; therefore requiring distinct production techniques. The first patent was acquired by Schelleng [2]. Hence, a lot of researches have been carried out which later create more attentions for many foundries like Novacast [3] and Sintercast [4] to have successfully produced CGI alloys using standard production methods such as thermal analysis system with good foundry techniques. CGI has been used to manufacture automotive diesel engines and an increase to improve the performance of the engine is still demanding but currently, the manufacture of gasoline engines using CGI is now emerging. However, the significance of CGI has been traced to its ability to fit into the trend of lightweight materials and this of course is as a result of cooling moduli and graphite morphology. This result in engines in some cases (cylinder block) having high fatigue properties, good elastic modulus and even lighter than engines made with aluminium and/or alloys that could reduce fuel consumption and emission [5].

It has been established that the effect of increasing nodularity does occur naturally due to increased cooling moduli or thin section of a casting [6]. Buska *et al.*, [7] established a manufacturing technological procedure for casting of CGI relating the chemical composition to microstructure analysis. The technology was able to meet the requirement on microstructure and mechanical properties of CGI for casting section thickness more than 16mm having consistent composition. A two-stage treatment process for producing CGI based on the reoxidation of Mg-treated melt was proposed by Suarez and Loper [8]. Their results showed that with no titanium addition, consistent and repetitive compacted graphite morphology can be achieved. Guzik *et al.*, [9] studied the use of Mg alloy in modern tundish plus cored wire injection method for the production of CGI and it was found that the method can produce high quality CGI of pealitic-ferritic matrix that is close to GJV 400 grade.

Gorny *et al.*, [10] addressed the effect of cooling rate and titanium addition on the microstructure and thermophysical parameters of thin walled graphite iron. It was concluded that the microstructure, graphite morphology and thermal conductivity of thin walled casting and as a function of temperature are largely influenced by cooling rate and titanium addition. Guesser and Martins [11] therefore, investigated the

optimisation of damping capacity and stiffness of high strength cast irons through alloying (Cu, Sn, Mo and Cr) elements and how these properties affect the microstructure. It was concluded that CGI was found to be intermediate for both LGI and SGI which in turn depend on the eutectic cells.

CGI or vermicular graphite iron has been known to provide good performance due to the consistent compacted graphite morphology. However, this material still remains a dormant material for industrial application. The reason being the narrowness of the stable range of CGI (Figure 1), making it difficult to ensure risk free production which poses very strict process control and in turn lead to large capital investment of control equipment [1,12]. Also, variations in composition and cleanliness of the charge materials make it impossible to achieve a fixed chemistry specification for CGI [1]. Therefore, the combinations of alloying elements at varying level still stand as the major detriment to achieving a correct and consistent compacted graphite morphology and matrix structure, which invariably results into negative effect on CGI properties. Based on the highlighted previous and recent studies, this research therefore intends to vary alloying elements require to produce CGI with optimum properties combination using rotary furnace.

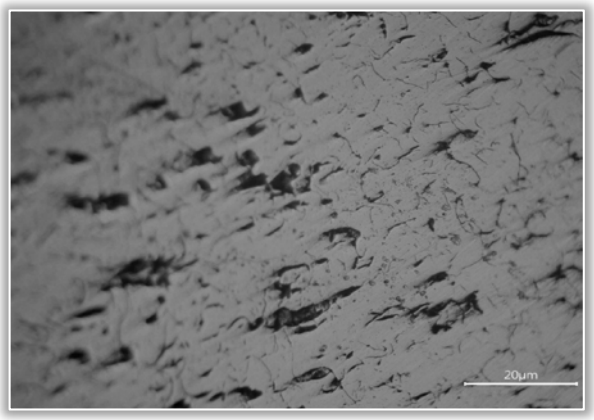

Fig. 1a: Microstructure of Unetched Alloy C at 200X

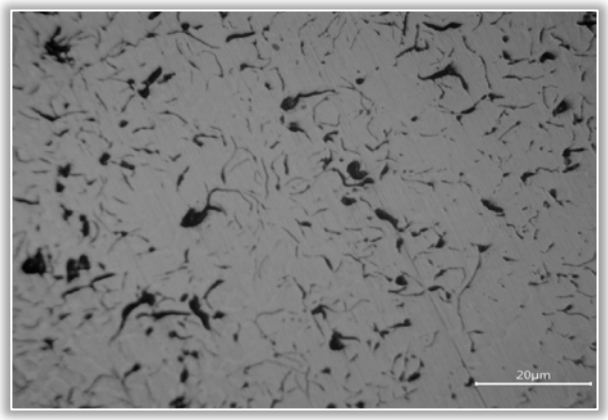

Fig. 1b: Microstructure of Unetched Alloy A1 at 200X

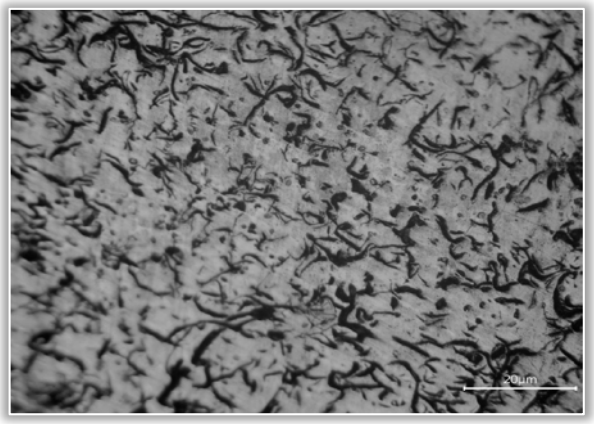

Fig. 1c: Microstructure of Unetched sample A2 at 200X

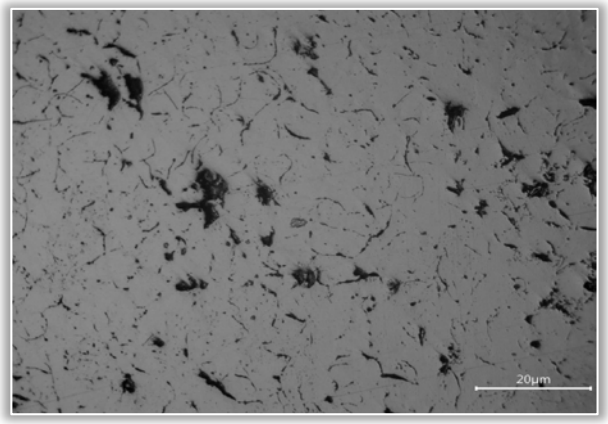

Fig. 1d: Microstructure of Unetched sample A3 at 200X

2. EXPERIMENTAL PROCEDURE

The materials used in this work are the grey iron, graphite, Ferrosilicon magnesium (FeSiMg), Cerium-based ferrosilicon alloy (FeSi alloy), aluminium, copper and antimony. The irons were melted and produced with a rotary furnace of 60 kg capacity. Four melts were poured with varying antimony addition and nearly fixed alloying elements addition. The chemical compositions of the grey iron and ferroalloys used are shown in Tables 1, 2 and 3.

The preheated aluminium Al, copper Cu and FeSi alloys of particle sizes in the range 0.2 to 0.7 mm were added to the ladle when tapping from the furnace to preheated/treatment ladle. The first melt was nodularized with FeSiMg only (C) without antimony. Second A1, third A2 and fourth A3 melts were nodularized, inoculated and treated with aluminium and copper and varying antimony addition.

The melt was superheated to about 1530 °C before being tapped into preheated ladle prior pouring. The melt was tapped into the pouring ladle at about 1470 °C after which the metal stream was treated with ferrosilicon alloys and later poured at about 1420 °C into the green sand mould in which cylindrical bar samples (C, A1, A2 and A3) with equal dimensions (Ø25 mm by 200 mm) were produced. The cylindrical bars cast were machined in order to determine the tensile strength, and sectioned to carry out hardness and microstructure of the alloys produced.

Chemical composition of the samples was examined by a spectrometer. The metallographic samples were prepared using standard procedures. This was done by sequence of grinding and polishing with 1µm particle size Alumina paste. Polished samples were etched in 2% nital for microscopic examinations using an optical microscope and the micrographs were analysed with imageJ software. The hardness test of the samples was done by using Rockwell hardness tester type A (HRA) with 60kgf (or 0.59KN) load.

Table 1: Chemical Composition of the Scrap Iron Used [8].

Elements	C	Si	Mn	P	S	Fe
Wt %	2.5-3.5	1.4-2.8	0.2-0.5	0.06-0.2	0.06-0.12	Remaining

Table 2: Elemental Analysis of the MgFeSi Alloy Used (Ceramic and Alloy Specialist (CAS) Pty Ltd)

Elements	Si	Mg	Ca	Al	Fe
Composition %	45 – 48	5.0	1.0	‹ 1.2	Balance

Table 3: Elemental Analysis of Ultraseed Ferrosilicon Alloy Used. (CAS Pty Ltd)

Elements	Si	Ca	Ce	Al
Composition %	72.5	1.13	1.8	1.01

Table 4: Chemical Analysis of Graphite Used.

% Carbon	% Sulphur	% Ash	% Volatile	% Moisture
66.0	0.57	30.20	3.10	0.10

3. RESULTS AND DISCUSSION

— Chemical Composition

Table 5: Treatment of Samples with Various Amounts in Weight Percent

Samples	Treatment (wt %)
C	5.0 MgFeSi alloy + 0.25 Ultraseed FeSi alloy
A1	5.0 MgFeSi + 0.25 Ultraseed FeSi alloy + 0.5 Al + 1.0 Cu + 0.0045 Sb
A2	5.0 MgFeSi + 0.25 Ultraseed FeSi alloy + 0.5 Al + 1.0 Cu + 0.0050 Sb
A3	5.0 MgFeSi + 0.25 Ultraseed FeSi alloy + 0.5 Al + 1.0 Cu + 0.0294 Sb

The chemistry of the samples produced as presented in Table 5 showed that the alloys solidified as both hypoeutectic (C, A1) and hypereutectic (A2, A3) CGI alloys. Hence, the CGI samples were obtained at a carbon equivalent (CE) range of 3.84% – 4.59%. This might be due to high melting temperature which influence the solidification rate (Singh, 2009) and of course causes the carbon and silicon to increase and decrease from C to A3 respectively. Meanwhile, all the CGI samples produced were influenced by both compactising and anti-compactising elements. Silicon and Magnesium showed an appreciable decrease ranging from (1.69 – 1.76) % and (0.02-0.036) % respectively. This however could be compared to Ce (0.022-0.035), Al (0.005 - 0.368), Cu (0.26 – 1.03) and Sb (‹0.002 – 0.0294) % contents respectively.

The variation in CE might be due to Si/C ratio (i.e. the lower the Si/C ratio, the higher the CE) and/or alloying elements such as Cu and Al which might decrease the carbon solubility during solidification (Konig, 2011). Therefore, the final chemistry of the CGI was mainly influenced by Sb, Al, Cu, Mg, Ce and consequently with CE.

Table 6: Chemical Analysis of the CGI Alloys Produced.

Iron Alloys	Average Chemical Composition (wt. %)										CE (%) Si/C		Mg /S
	C	Si	Mn	P	S	Al	Cu	Mg	Ce	Sb			
C	3.22	1.76	0.252	0.109	0.139	0.005	0.26	0.036	0.022	‹0.002	3.84	0.55	0.29
A1	3.53	1.69	0.238	0.149	0.141	0.313	1.02	0.020	0.029	0.0045	4.14	0.48	0.12
A2	3.75	1.75	0.269	0.211	0.110	0.368	1.03	0.032	0.034	0.0050	4.40	0.47	0.29
A3	3.96	1.69	0.261	0.197	0.147	0.352	1.02	0.025	0.035	0.0294	4.59	0.43	0.17

*CE = % $C + {}^{1}/_{3}$ (Si + P)% (Singh, 2009)

Table 5 also presents the Mg/S ratio for each of the alloy produced. This is an important factor for chemical composition of the CGI [13]. The Mg/S values are within the range of (0.12 – 0.29) as the values imply the degree at which magnesium react with sulphur and the level at which sulphur is free. Hence, the maximum ratio recorded in this work is smaller to the value reported by Alkan [14]. Despite the lower Mg/S, the final chemistry of the CGI alloys produced still an appreciable amount of Mg of which varies as a result of differing melting temperature and holding time which eventually make it faded away [15].

— Microstructure

The microstructure details of etched (graphite morphology, matrix structure) and the analysed contents of the microstructures (amounts of phases, nodule count and/or % nodularity) of the CGI alloys produced are presented in Figures 1 – 3 and Table 7. Figure 2a shows the micrograph of sample alloy C. From the micrograph, it was revealed that the alloy consisted of compacted graphite (CG) particles which were thick, short and worm-like with round–ended edges as well as graphite particles in form of nodules as in Figure 3a.

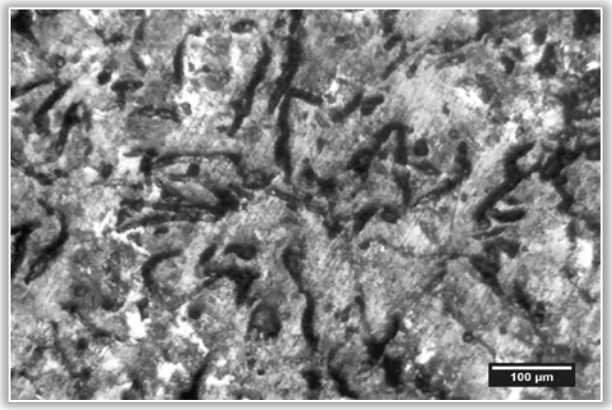

Fig.2a: Microstructure of Etched Alloy C at 200X

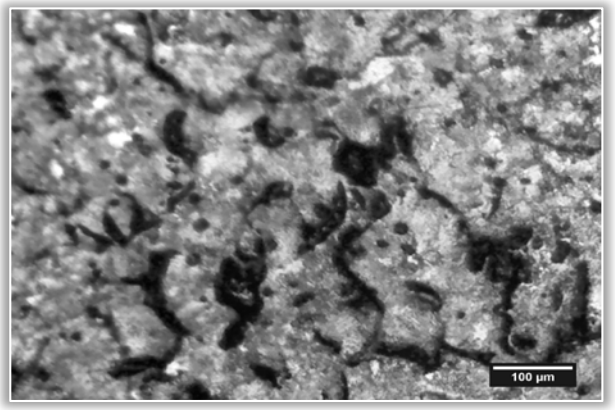

Fig.2b: Microstructure of Etched Alloy A1 at 200X

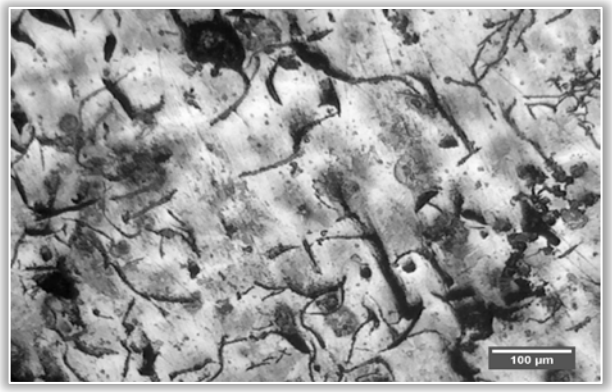

Fig.2c: Microstructure of Etched A2 at 200X

Fig.2d: Microstructure of Etched Alloy A3 at 200X

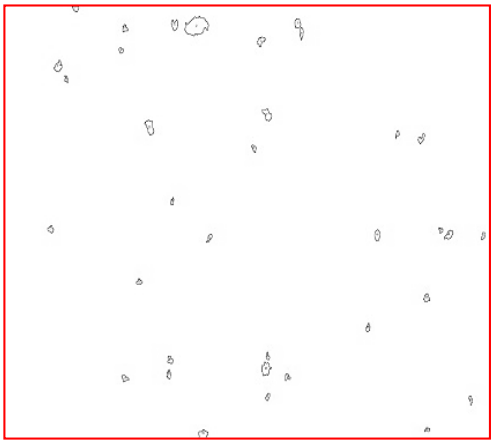

Fig.3a: Spheroidal Graphite Particles for Alloy C

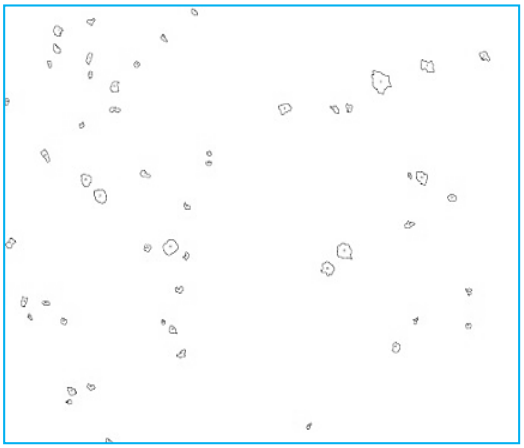

Fig.3b: Spheroidal Graphite Particles for Alloy A1

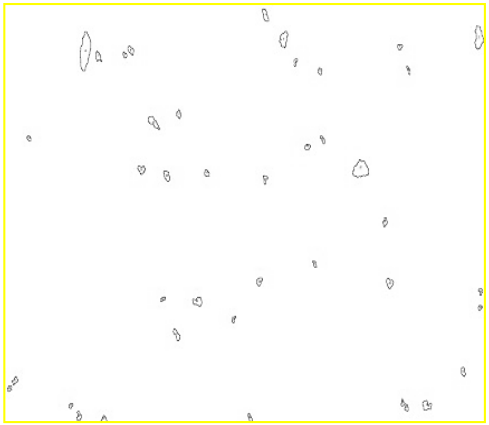

Fig.3c: Spheroidal Graphite Particles for Alloy A2

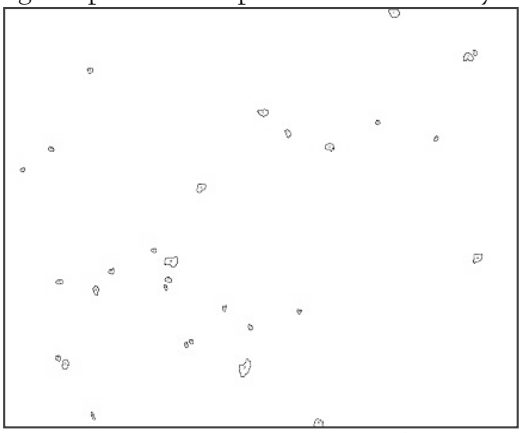

Fig.3d: Spheroidal Graphite Particles for Alloy A3

Table 7: Graphite Particles and Matrix Analyses using Image Analyzer.

CGI Alloys	Nodule Count/mm^2	% Nodularity	% CG	% Pearlite Area
C	35	24.5	75.5	88
A1	53	30.3	69.7	77
A2	41	27.2	72.8	94
A3	30	22.6	77.4	90

These graphite particles were embedded in pearlitic structure with interspersed nodules. The obtained structure was due to the addition of Mg in form of alloy at an insufficient amount that will not form full spheroidal graphite. Meanwhile, the microstructure showed few traces of carbide content. The carbide content might be due mainly to low Si content (1.76%) and/or high S amount (0.139%) and casting process of the CGI alloy. However, the pearlitic matrix (80%) and the high number of nodules (35) were as a result of residual Mg. This is true as it corroborates with the report of Konig [16].

Figure 2b which showed the microstructure analysis of sample alloy A1 to consists of CG having thick, short and wormy like graphite particles co-existing with number of nodules as in Figure 3b and Table 7 which are evenly distributed within the CG. The CG and SG are embedded in pearlitic matrix with few traces of carbides. However, it must be noted that the CG particles was observed to have emanated from the SGI nucleation and growth mechanism [17,18] as this was more obvious and pronounced in the obtained micrograph (microstructure) of sample alloy A1 compared to sample alloy C. Hence, the addition of Al and Cu influence the graphite particles and most importantly the matrix structure by ensuring the formation of pearlitic structure [19]. Meanwhile, the eutectic carbide amount of sample alloy A1 were more than sample alloy C as analysed. The reason for this might be due to the high level of phosphorus (P), sulphur (S) contents and low amount of silicon (Si) (i.e. lower Si/C ratio as shown in Table 4.1) [20-23] coupled with the casting process. But the combined effect of both the nodulariser and inoculants (which ought to have increased the Si content thereby giving room for more ferrite promotion) was able to solidify a CG. Sample alloy A1 was able to form CG with more regular graphite nodules. The higher number of nodules and nodularity could be as a result of the cooling rate coupled with other alloying elements. Also, the presence of Sb content was approximately within the recommended range for SGI [24], as this showed no negative effect rather beneficial as regard number of nodules.

Figure 2c showed the microstructure of the sample alloy A2. It was observed that the CG showed a few complex coral-like appearances or crab-like graphite embedded in pearlitic matrix of which contained more (smaller) nodules than samples alloys C and A3 as in Figure 3c and Table 7. Sample alloy A3, as shown in Figure 2d revealed few CG with needle-like edges with combination of thin, thicker, shorter and wormy-like morphology. The reduction in the number of nodules and/or nodularity of sample alloy A3 could be associated with the high sulphur content (0.147%) as this tends to reduce the formation of nodular graphite particles. This observation is similar to the report given in ASM Metals Handbook [25].

Generally, it was observed that the CGI alloy (C) had the intermediate amount of CG with better morphology and distribution and lower amount of SG as presented in Figure 3 than sample alloy A1 respectively. As a result, the nodularity of A1 is higher than C. However, the Sb being in sample A1 affected the morphology of the CG as it revealed traces of very few fairly needle-like edges. Also, the matrix structures of the CGI alloys were observed to have been influenced by the segregation of alloying elements added [16]. Figures 1 and 2 revealed that the Sb addition increased the crab graphite and/or complex coral- like graphite particles and this was as a result of excess residual amount of Mg and Ce [26]. Also, increasing the Sb addition causes the graphite particles to be embedded more in pearlite than ferrite phases and this increment was able to curve and bend the CG particles with needle – like edges [17]. These observations can be seen in sample A2 and this could be as a result of the high amount of Cu and Al which caused larger amount of thinner CG graphite to be pronounced, this however is similar to the report of Chen and Chen [27] and the findings of Yuichi *et al.*, [28]. Meanwhile, Sb addition (0.0045%) was able to form regular CG morphology particularly for sample alloy A1.

— Tensile Strength Analysis

The result of the universal tensile strength (UTS) for all CGI alloys produced is presented in Figure 4.

Figure 4 showed the result of the UTS for CGI alloys produced. It was observed that the strength of the CGI alloys C and A1, showed a decreasing trend. Comparatively, there was an increase in the strength of Sb – modified CGI alloys for A2 and A3 with UTS values of 327 MPa and 316 MPa respectively. Hence, the UTS results could be justified by the chemical analysis of produced alloys mainly by CE as shown in Figure 6, %Mn, % S and % P of the Sb–modified CGI alloys. It must be noted that, the UTS values of samples A2 and A3 correspond with their respective hardness values (Figure 5) which in turn corroborate with the Sb additions as presented in Figure 7. Despite the obtained gas porosity defects that was revealed, the analysed results of the nodule count, % nodularity and matrix amount (% pearlite) by area, did correlate with the UTS results of

Sb–modified CGI alloys particularly for samples A2 and A3 as presented in Table 7. However, this defect posed a negative effect on the UTS of alloys C and A1 respectively coupled with the appearance of the eutectic carbides. The distribution of the graphite particles, graphite morphology and embodiment of graphite particles in the matrix were among factors that influence the tensile strength of the produced CGI [29-31].

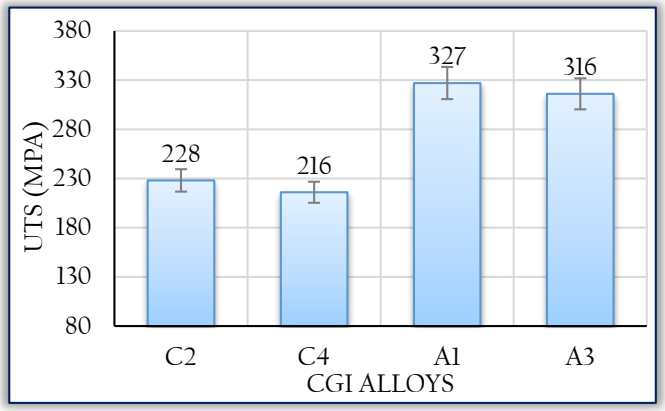

Figure 4: Ultimate Tensile Strength of the CGI Alloys Produced

— Hardness Test Analysis

Figure 5 presented the hardness property of the cylindrical bar samples of CGI alloys produced. Figure 5 showed the result of the average hardness value (HRA) of all CGI alloys produced. It was observed that the sample alloy C recorded the highest hardness value of 87.4 HRA while, the least value was obtained by sample alloy A1 (83.2 HRA). Meanwhile, the intermediate result was achieved by sample alloy A2 with hardness value of 86.9 HRA. Hence, the result of the hardness corresponds with the chemical analysis obtained and microstructure analysed.

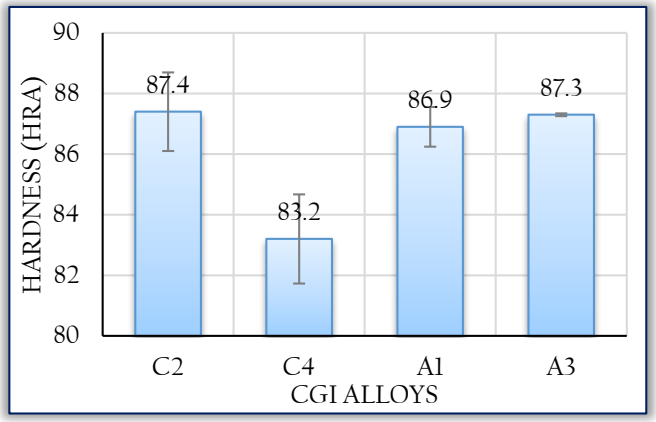

Figure 5: Hardness Result of CGI Alloys

— Effects of CE analysis on UTS and Hardness

Figure 6 showed the relationship between the UTS and the CE of CGI alloys produced. However, it was observed that the UTS and hardness of the alloy decreases from C to A1 as then increases from A1 to A3 as the alloys showed increase in the CE values as shown in Figure 6. This behaviour could be related to the discussion presented in Section 3.2 [32, 33]; that the values of hardness increased as the CE values decreased and vice versa. Also, the hardness result is akin to the result of the UTS in the same trend. Generally, it was observed in Figure 6 that an increase in hardness value followed a decrease in carbon equivalent. That is, alloys that solidified within hypoeutectic range possessed higher hardness compared to those alloys which solidified within slightly and/or strongly hypereutectic range.

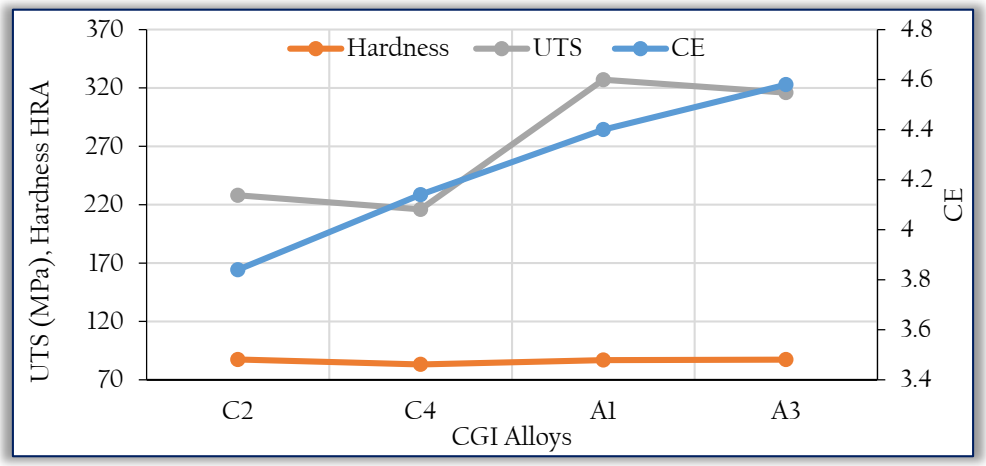

Figure 6: Relationship between UTS, Hardness and CE of CGI Alloys

— Effects of antimony on UTS and Hardness

It is observed from Figure 7 that increasing antimony addition increases the UTS value of the alloys with variations in the trend.

Despite Sb addition with constant addition of Cu amounts, the structure however still manifested few ferrite phases for alloy sample A2. The reason for this might be due to CE value, % S and high amount of Al which was able to decrease the carbon solubility [34, 35], as this increased the degree of graphitization from 0.24% to 2.8% Al [36]. The occurrence of ferrite might be due to the segregation of the alloying elements which influence both nucleation and growth of ferrite. Hence, it is noted that as antimony addition increases in Sb –

modified CGI the tensile strength decreases as shown in Figure 7 and 8. Comparing sample alloy C to Sb-modified alloys, the CE values of these alloys showed that it solidified as hypereutectic with sample alloy C which possessed the highest hardness value (87.4 HRA) and this is due to the fact that it solidified as least hypoeutectic iron alloy. However, it was observed that the antimony addition might have influenced the hardness results as presented in Figure 8. Despite low CE of the sample alloys, the addition of Sb showcased an increase in the hardness values. That is, as Sb increased, the hardness increased while the tensile strength increased to certain limits which as well depend on the chemical composition of the alloys [37, 38].

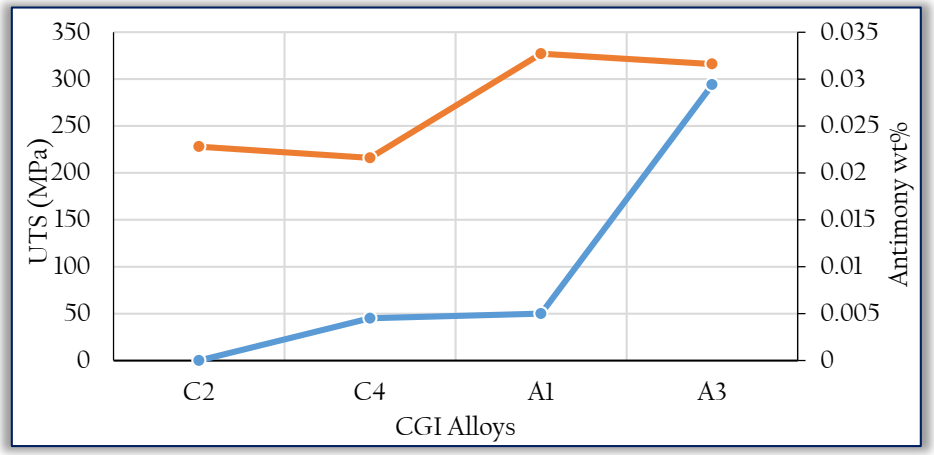

Figure 7: Variation of Antimony with Hardness of Sb-Modified CGI Alloys

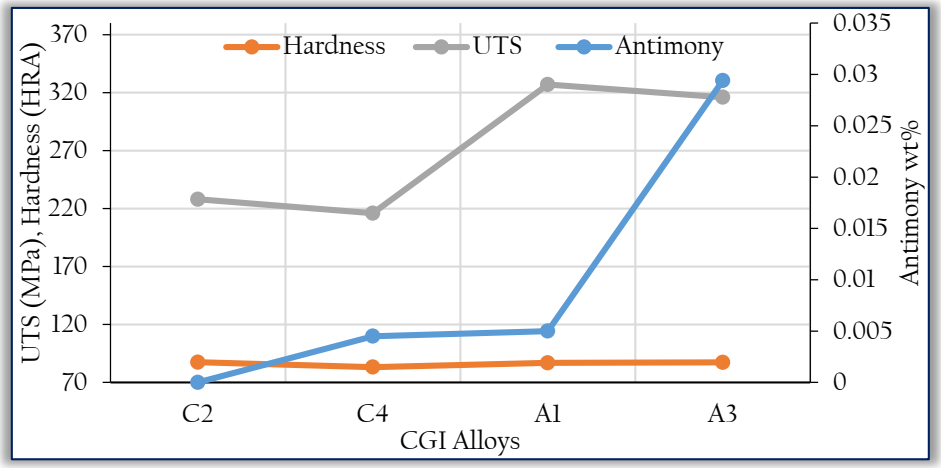

Figure 8: Relationship between Antimony Hardness and UTS for Sb – Modified CGI Alloys Produced.

— Effects of % elongation on UTS and Hardness

Figure 9 described the relationship between the UTS and the percent elongation of the CGI alloys produced. It has been established that the strength of cast irons increases with increase in pearlite content and with a decrease in % elongation [39] depending majorly on the alloying elements present either as pearlite promoter or carbide stabilizer [13]. Hence, it was observed in Figure 10 that as the UTS decreases for sample alloy C – A1, the %Elongation increases with increasing nodule count and/or nodularity. So also, the behaviour of sample alloys A2 and A3 followed the same trend. It is interesting to note that despite higher UTS value of sampleA1, it still possessed the highest amount of ductility (as this is a result of few ferrite areas). Generally, it was observed from Figure 10 that the alloys showed increase in ductility, decrease in UTS with increase in hardness for Sb-modified CGI alloy A3 except for sample alloy A2 which showed an increase in all the related properties. Whereas, the unmodified CGI alloy C showed a decrease in UTS, increase in ductility with decrease in hardness.

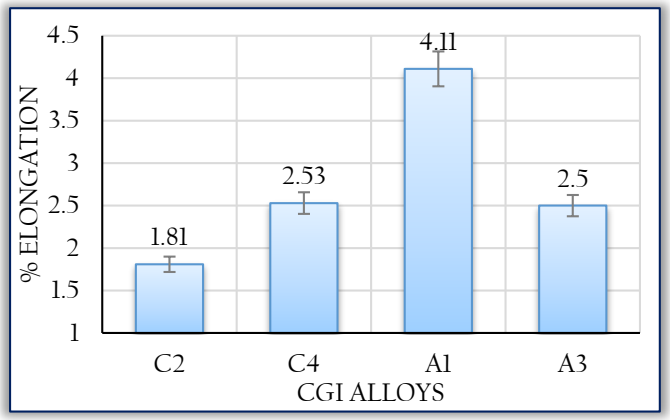

Figure 9: % Elongation of the Produced CGI Alloys

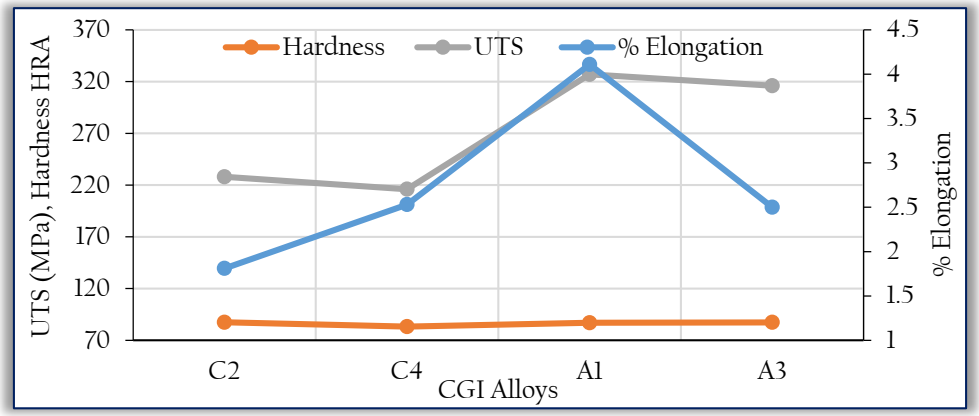

Figure 10: Relationship between UTS, Hardness and % Elongation of all CGI Produced.

— Effect of Nodularity and Pearlite content on UTS

Figure 11 described the relationship between UTS, Pearlite and Nodularity of the CGI alloys produced.

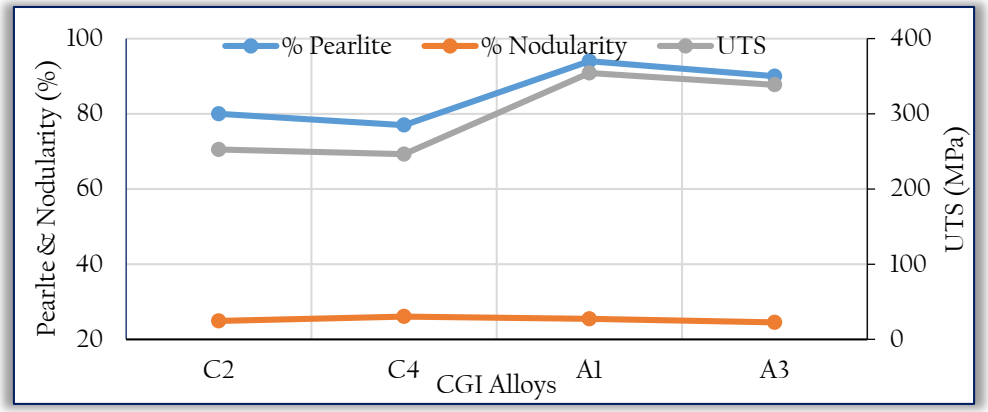

Figure 11: Effect of Pearlite and Nodularity Content on the Strength of Sb – Modified CGI Alloys

Figure 11 showed that decreasing pearlite content in Sb- modified CGI causes increase in tensile strength of the alloy for sample A1. This agreed with the work of Bockus [37] which reported that as antimony helps to modify the microstructure, the pearlite content in the matrix decreased with increasing carbon equivalent. Meanwhile, it was reported by Yuishi *et al* [28] that combination of Sb and Ce resulted into full pearlitic structure and significantly increased hardness and strength as this true for sample alloy A2. Therefore, the result of the UTS is in consonance with the microstructure details especially within and/or between unmodified and Sb – modified CGI.

There are many factors that influence higher nodularity of CGI, among these factors are; magnesium content, post inoculation and cooling rate [13]. It was observed in Figure 11 and from Tables 6 and 7 that as the Mg/S level increases the % nodularity increases with increase in tensile strength. It must also be noted that increase in Mg/S level increases the pearlite content with increase in tensile strength and nodularity. It also appeared that Si/C ratio influenced the nodularity of the alloys such that the alloys with highest Si/C possessed the larger amount of nodularity as in Table 6 and 7. However, the melt temperature, holding time and cooling rate might also affect the nodularity though the literature has been uncertain about these.

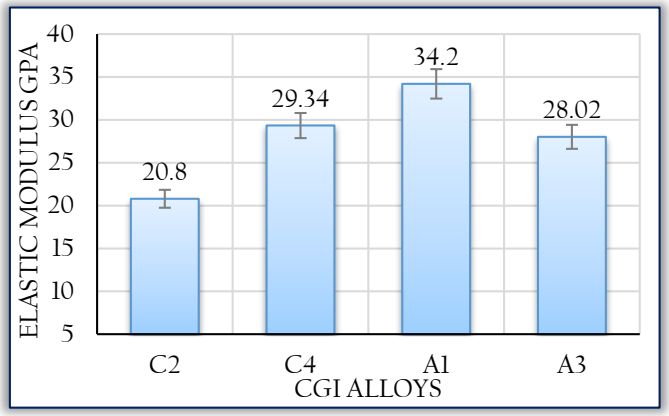

Figure 12: Elastic Modulus of the CGI Alloys Produced

— Elastic Modulus Analysis

The result of the elastic modulus (E-modulus) for all CGI produced and its relationship to % nodularity and pearlite is presented in Figures 12 and 13. It was observed in Figure 12 that sample alloy A2 had the highest E – modulus (34.2 GPa) while sample alloy C was the least (20.8 GPa). There was a variation in the elastic modulus for CGI samples (C to A3) as it showed an increasing trend with increase in the Sb addition up to

certain limit. This behaviour could be likened to the amounts of nodules (nodule count) and/or nodularity of the alloy because the elastic modulus increases with increasing nodularity and decreases with decreasing pearlite content. This is in accordance with work studied by Sintercast and Alkan [6,15] and this was only true between samples alloys A2 and A3 as these showed a consistent trend despite higher nodularity obtained in sample alloy A1 (Figure 13). The reason for the reduction in their elastic modulus might be due to the higher amount of thinner graphite particles revealed in their structure. This is akin to the report of Chen and Chen [27]. However, the result of the E- modulus could be related with UTS and % elongation for samples alloys C and A1.

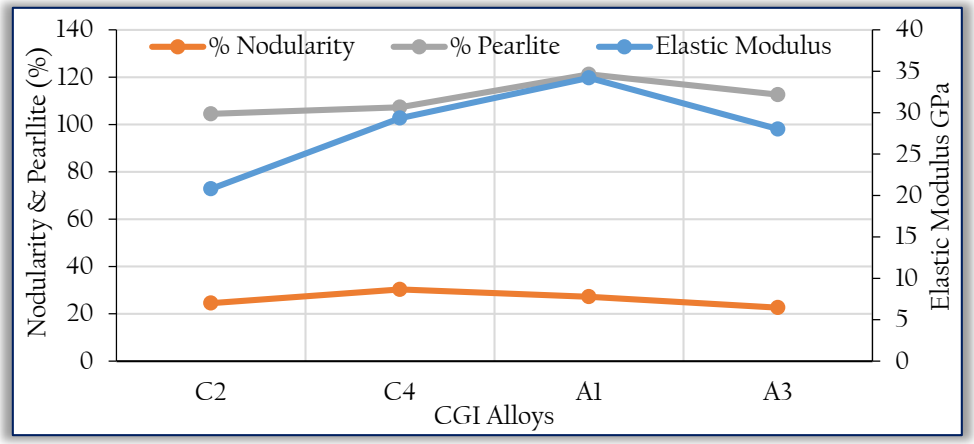

Figure 13: Elastic Modulus of the CGI Alloys Produced

4. CONCLUSIONS

In the work, production of compacted graphite iron (CGI) with the use of rotary furnace was achieved. Therefore, the following conclusions are drawn;

a) Despite variations obtained in the chemistry of all the alloys particularly high sulphur content and low silicon content, compacted graphite irons were produced.
b) Optimum results are achieved when carbon equivalent (CE) is at 4.4.
c) Antimony (Sb) addition was observed to have modified the graphite morphology of compacted graphite from thick and wormy – like with round –ended edges to less thick and worm – like with needle – like end having rough edges (or spikes).
d) The ferrite appearance was observed in the Sb – modified CGI structure due to the segregation of alloying elements and despite, the tensile strength was improved.
e) The appearance of eutectic carbide caused a decrease in the UTS and % Elongation.
f) The effect of Cu and Sb could not be well ascertained and this might be due to level of Al contents (i.e. 0.3 – 0.4) % Al.
g) Sb addition (0.005 – 0.029) % with Al and Cu contents of 0.3% and 1.0% could not increase the pearlite amount rather enhance carbide content. This range showed decreasing trend in the tensile strength and % nodularity (depending on the Mg/S ratio) but was able to increase the hardness of the CGI alloys respectively.
h) Sb addition ranging from 0.0045 – 0.005% was able to increase nodularity and strength.
i) Generally, the Sb – modified CGI showed better mechanical properties than the unmodified CGI alloys respectively.
j) Of all the CGI samples produced, samples alloys A2 and A3 experienced better results with sample A2 having the optimum results.
k) Therefore, depending on the alloying element applied, CGI can be produced with varying chemistry which invariably still possessed close results in terms of graphite morphology and mechanical properties.

References

[1] Subrata, C., (2003). Manufacturing and Application of CGI. The Institute of Indian Foundrymen, 66th Indian Congress. Pp. 4-12.
[2] Dawson, S., (1999). Compacted Graphite Iron- Mechanical and Physical Properties for Engine Design. *Materials in Powertrain Conference* (Werkstoff und Automobilantrieb), VDI, Dresden, Germany. Pp. 1-19.
[3] Novacast, 2014. http://novacast.se/
[4] Sintercast, (2014). http://www.sintercast.com/technology
[5] Guesser, W. L., (2009). Propriedades Mecânicas dos Ferros Fundidos. *Ed Edgard Blücher*. Pp.12-25.
[6] Sintercast, (2012). Compacted Graphite Iron – Mechanical and Physical Properties for Engine Design. *Sintercast*. Pp. 1-20.

[7] Bouska, O., Heunisch, J., Zadera, A., Nedelova, K. and Kobersky, F., (2012). Development of a Manufacturing Technology of Compacted Graphite Iron Castings from a Cupola Furnace. *Archives of Foundry Engineering*. ISSN (1897-3310). Vol. 12 (1). Pp. 125-129.
[8] Suarez, O. M. and Loper Jr., C. R., (2001). Production of Compacted Graphite Irons through Two-Step Treatment Method. *Metallurgical Science and Technology*. Pp. 25-31.
[9] Guzik, E., Kopycińskia, D., Kleingartnerb, T. and Sokolnickic, M., (2012). The Structure and Mechanical Properties of Pearlitic-Ferritic Vermicular Cast Iron. *Archives of Foundry Engineering*. ISSN (1897-3310). Vol. 12 (1). Pp. 33-36.
[10] Gorny, M., Lelito, J., Kawalec, M. and Sikora, G., (2015). Thermal Conductivity of Thin Walled Compacted Graphite Iron Castings. *ISIJ International*, Vol. 55, No. 9, pp. 1925–1931.
[11] Guesser, W.L. and Martins, L.P.R., (2016). Stiffness and Vibration Damping Capacity of High Strength Cast Irons. *SAE International*. Pp. 2-6.
[12] Singh, V., (2009). Physical Metallurgy. Standard Publishers Distribution, 1705 Nai Sarak, New Delhi-110006. Pp. 446-463.
[13] König, M., (2011). Microstructure Formation during Solidification and Solid State Transformation in Compacted Graphite Iron. *Dissertation., Charmers University of technology*, Sweden. Pp. 2 – 3, 9 – 12.
[14] Reese, C. R. and Evans, W. J. (1998). "Development of an In the Mold Treatment Process for Compacted Graphite Iron Cylinder Blocks". *AFS Transactions*. Pp. 673 - 683.
[15] Alkan, A. (2011). Production and Assessment of Compacted Graphite Iron Diesel Engine Blocks. M. Sc. Thesis Dissertation. Middle East Technical University.
[16] Http://www.sintercast.com/file/process-control-for-the-reliable-high-volume-production-of-compacted-graphite-iron-3.pdf , 2013-06-14
[17] Theuwissen, K., Lacaze, J and Laffont, L (2016). Structure of Graphite Precipitates in Cast Iron. Journal of Carbon, Elsevier. Vol. 96, Pp. 1120 – 1128.
[18] Dawson, S., (2002). Process Control for the Production of Compacted Graphite Iron. *American Foundry Society*, Pp. 32-43.
[19] Sugwon K., Cockcroft, S. L., Omran, A. M. and Honam H. (2009), ''Mechanical, Wear and Heat Exposure Properties of Compacted Graphite Cast Iron at Elevated Temperatures'', Journal of Alloys and Compounds. Pp. 253 - 256.
[20] Saka S. O., Seidu S. O., Taiwo A. S and Riposan I.: Chilling Effect of Iron Powder on the Microstructure and Hardness Property of Strongly Hypereutectic Grey Cast Iron. Annals Faculty of Engineering, Hunedoara, Int. J. Engineering, Vol. 17 Issue 4, Pp 13 – 22, 2019.
[21] Seidu S.O and Ogunniyi I. O. (2012). Control of Chilling Tendency in Grey Cast Iron Reuse. Material Research. Vol.16, No.1 ISSN 1516-1439. Pp. 2 – 5.
[22] Stan, S., Chisamera, M. and Riposan, I. (2009). Solidification Pattern of Hypoeutectic Grey Cast Iron in Wedge Test Samples, POLITEHNICA University of Bucharest, Romania, Metallurgical International, Vol. XIV, special issue No. 2. Pp 27-29.
[23] American Society for Testing of Materials, ASTM, (2000). ASTM. *Standard A367-60*: Standard Test Methods of Chill Testing of Cast Iron. West Conshohocken. p. 151.
[24] Aborn, R. H. (1976). What Antimony may do for you in Gray and Ductile Iron, *AFS Transactions* 76-75, pp. 503 - 506.
[25] ASM Metals Handbook, (1985). American Society for Metals (ASM), Metals Park, Ohio, USA.
[26] Foundrymen's Guide to Ductile iron Microstructure. (1984). Effect of alloying and subversive elements. Section IV. Pp. 61 – 71.
[27] Chen, J.K. and Chen, S.F., (2011). Thermal Conductivity of an in-Situ Metal Matrix Composite - Cast Iron, Metal, Ceramic and Polymeric Composites for Various Uses, Dr. John Cuppoletti (Ed.), ISBN: 978-953-307-353-8. *InTech*, Vol. 10. Pp.212-223.
[28] Yuichi, T and Mikio, F. (1985). Effect of Silicon and Antimony Addition on Graphite, Matrix Structure in Compacted/Vermicular Graphite Cast Iron. Pp. 149 – 155
[29] Elin, N., (2014). Relation between Microstructure Features, Cooling Curves and Mechanical Properties in CGI-cylinder Block. Master of Science Thesis in Material Science. Stockholm, Sweden. Pp. 7-8.
[30] Stan, S., Chisamera, M., Riposan, I., Ivan N., and Barstow, M. (2012). Iron Powder Treated Gray Irons: Critical Shape Characteristics for Graphite Nuclei. Journal of Materials Engineering and Performance, Vol. 21(8), Pp. 1792-1795.
[31] Dawson, S., Hollinger I., Robbins, M., Da'eth, J., Reuter, U., and Schmidt, H. (2001). The Effect of Metallurgical Variables on the Machinability of Compacted Graphite Iron. *SAE International Congress, Detroit*. Pp. 4-59.
[32] Stefanescu, D. M. (1989).Classification and Basic Metallurgy of Cast Iron, Metals Handbook, Vol. 1, 10th Ed. ASM International, Materials Park Ohio, USA. Pp. 4-7.
[33] Sergeant, G. F. and Evans, E.R., (1978). Production and Properties of Compacted Graphite Irons. *BCIRA Publication*. p. 115.
[34] Soiński, M. S., Susek, P., Hübner, K. and Mierzwa, P. (2008). The Low-Aluminium Cast Iron of Reduced Silicon Content Treated with Cerium Mischmetal. Archives of Foundry Engineering. 8(2), Pp. 123-128.
[35] Bobro, J. G. (1976). Particularités de la structure et des proprieties des fonts á l'aluminium. In: *43rd International Foundry Congres*. Bucurest. (26). p. 146.
[36] Neumann, F., Schenck, H., Patterson, W., (1959). Eisen- Kohlenstoff-Legierungen in thermodynamiccher Betrachtung. *Giesserei. Tech.-Wissen.* (23), 1217-1246, 1339.
[37] Bockus, S. (2006). A Study of the Microstructure and Mechanical Properties of Continuously Cast Iron Products. METABK 45 (4) pp. 287-290. *Foundry Engineering*. Vol. 7, Issue 3. Pp 183 – 186.
[38] Liu, Z., Chen, W. and Du, Y., (2012). Influence of Cooling Rate on Antimony Addition Content on Graphite Morphology and Mechanical Properties of a Ductile Iron. *China Foundry*, Vol. 9(2): Pp 114-118.
[39] Dawson, S. and Schroeder, T., (2000). Compacted Graphite Iron: A Viable Alternative. Engineering Casting Solutions AFS. Pp.1-8.